Surface Tension Transport of Prey by Feeding Shorebirds: The Capillary Ratchet

Manu Prakash, *et al.*

Science **320**, 931 (2008);
DOI: 10.1126/science.1156023

throughout tropical South America, fed exclusively on female flowers, and, in all but one locality, fed on a single species of host (Fig. 1 and fig. S4). Other species (e.g., sp. 27) fed almost exclusively on female flowers (30 of 32 specimens) of at least two host species in Central America, but commonly fed on male ($N = 4$) and female ($N = 4$) flowers in areas west of the Andes in Ecuador (Fig. 1 and fig. S6). These variable patterns of host use form a mosaic that varies from community to community across large geographic areas (*20*) and complicates attempts to extrapolate local samples to global estimates of tropical diversity (*21*).

Although we report diversity exceeding the original morphological estimates by an order of magnitude (*15*), this must underrepresent the actual diversity of this group because our criterion for species delimitation is highly conservative (*15*). This is because we used a 4% mtCOI divergence, whereas other studies recognize species differing by less than 1% (*8*). As a result of this conservative criterion, we may be lumping biologically distinct species together, and single generalist species may actually represent multiple host-specific species (e.g., sympatric monophyletic lineages feeding on separate hosts; see sp. 37 in French Guiana, Fig. 1 and fig. S8). Also, our samples are limited; most of our collections were made during single trips, and our samples were restricted to species in fruit or flower at that time (table S1). Finally, the number of fly species recorded for a particular host plant species was most likely limited because the number of insect species detected rose as the number of collection localities increased (Fig. 3).

We also found that the distribution of hosts may also predict herbivore diversity at both local and regional scales (*6*, *7*). The neotropics include a mosaic of biogeographic zones reflecting a long history of repeated habitat fragmentation (*22*). During periods of habitat fragmentation, insect populations may be more likely than these plant populations to diverge, as insects have shorter generation times and can evolve more quickly than plants with long generation times (*15*). Furthermore, sexual selection accelerates rates of evolution in insects, particularly in groups with complex courtship displays such as *Blepharoneura* (*9*, *18*, *23*). When these new species come together, as habitats expand and host populations rejoin, assemblages of highly host-specific cryptic species result. In local assemblages of *Blepharoneura* (Fig. 1), the minimum pairwise divergence among sympatric species is ~6%, which suggests that they diverged at least 2.6 million years ago (*24*). During the past 2.6 million years, even seemingly uniform habitats experienced multiple cycles of fragmentation and expansion (*22*). If host plants represent "hard boundaries" (*25*) for ranges of host-specific insects, simple neutral models incorporating changes in habitat area (*25*) as well as time (*26*, *27*) could help account for patterns of diversity. Conflicting assessments of host specificity and diversity in the tropics (*2*, *3*, *28*) may reflect differences in geographic scale rather than differences in evolutionary or ecological processes.

References and Notes

1. R. M. May, *Philos. Trans. R. Soc. London Ser. B* **330**, 293 (1990).
2. V. Novotny *et al.*, *Science* **313**, 1115 (2006); published online 13 July 2006 (10.1126/science.1129237).
3. L. A. Dyer *et al.*, *Nature* **448**, 696 (2007).
4. I. S. Winkler, C. Mitter, in *Specialization, Speciation, and Radiation: The Evolutionary Biology of Herbivorous Insects*, K. J. Tilmon, Ed. (Univ. of California Press, Berkeley, CA, 2008), pp. 240–263.
5. T. Hunt *et al.*, *Science* **318**, 1913 (2007).
6. T. R. E. Southwood, *J. Anim. Ecol.* **30**, 1 (1961).
7. H. V. Cornell, *Ecology* **66**, 1247 (1985).
8. P. D. Hebert, E. H. Penton, J. H. Burns, D. H. Janzen, W. Hallwachs, *Proc. Natl. Acad. Sci. U.S.A.* **101**, 14812 (2004).
9. D. Bickford *et al.*, *Trends Ecol. Evol.* **22**, 148 (2006).
10. J. O. Stireman, J. D. Nason, S. B. Heard, *Evolution* **59**, 2573 (2005).
11. J. B. Joy, B. J. Crespi, *Evolution* **61**, 784 (2007).
12. H. C. T. Godfray, O. T. Lewis, J. Memmott, *Philos. Trans. R. Soc. London Ser. B* **354**, 1811 (1999).
13. V. Novotny, A. R. Clarke, R. A. I. Drew, S. Balagawi, B. Clifford, *J. Trop. Ecol.* **21**, 67 (2005).
14. M. A. Condon, G. J. Steck, *Biol. J. Linn. Soc.* **60**, 443 (1997).
15. See supporting material on *Science* Online.
16. M. A. Condon, L. E. Gilbert, *Am. J. Bot.* **75**, 875 (1988).
17. D. J. Funk, K. E. Omland, *Annu. Rev. Ecol. Evol. Syst.* **34**, 397 (2003).
18. M. A. Condon *et al.*, *Biol. J. Linn. Soc.* **93**, 779 (2008).
19. D. A. Norton, R. K. Didham, *Science* **315**, 1666b (2007).
20. J. N. Thompson, *The Geographic Mosaic of Coevolution* (Univ. of Chicago Press, Chicago, 2005).
21. C. D. Thomas, *Nature* **347**, 237 (1990).
22. J. Cracraft, R. O. Prum, *Evolution* **42**, 603 (1988).
23. T. C. Mendelson, K. L. Shaw, *Nature* **433**, 375 (2005).
24. We used Brower's (*29*) calibration of 2.3% (pairwise divergence) MY-1, which is used as the standard mitochondrial molecular clock estimate (*27*).
25. R. K. Colwell, D. C. Lees, *Trends Ecol. Evol.* **15**, 70 (2000).
26. S. P. Hubbell, *The Unified Neutral Theory of Biodiversity and Biogeography* (Princeton Univ. Press, Princeton, NJ, 2001).
27. M. A. McPeek, J. M. Brown, *Am. Nat.* **169**, E97 (2007).
28. V. Novotny *et al.*, *Nature* **448**, 692 (2007).
29. A. V. Z. Brower, *Proc. Natl. Acad. Sci. U.S.A.* **91**, 6491 (1994).

30. We thank many colleagues and students for assistance; museums and governmental agencies in Bolivia, Costa Rica, Ecuador, French Guiana, Peru, the United States, and Venezuela for assistance and permission to carry out the study; and D. C. Adams, D. J. Futuyma, D. H. Feener, L. E. Gilbert, S. H. McKamey, C. Mitter, A. L. Norrbom, M. C. Singer, and I. S. Winkler for helpful comments on the manuscript. Supported by the Smithsonian Institution, NSF, Hofstra University, Ithaca College, and Cornell College. Sequences of *Blepharoneura* specimens have been deposited in GenBank (accession numbers EF531751 to EF531769, EF531789 to EF531828, EF531890, EF531891, EU601764 to EU60230, and EU623470).

Supporting Online Material

www.sciencemag.org/cgi/content/full/320/5878/928/DC1
Materials and Methods
Figs. S1 to S10
Tables S1 and S2
Appendices S1 and S2

29 January 2008; accepted 9 April 2008
10.1126/science.1155832

Surface Tension Transport of Prey by Feeding Shorebirds: The Capillary Ratchet

Manu Prakash,[1] David Quéré,[2] John W. M. Bush[3]

The variability of bird beak morphology reflects diverse foraging strategies. One such feeding mechanism in shorebirds involves surface tension–induced transport of prey in millimetric droplets: By repeatedly opening and closing its beak in a tweezering motion, the bird moves the drop from the tip of its beak to its mouth in a stepwise ratcheting fashion. We have analyzed the subtle physical mechanism responsible for drop transport and demonstrated experimentally that the beak geometry and the dynamics of tweezering may be tuned to optimize transport efficiency. We also highlight the critical dependence of the capillary ratchet on the beak's wetting properties, thus making clear the vulnerability of capillary feeders to surface pollutants.

Phalaropes (Fig. 1A) and several other shorebirds with long thin beaks feed primarily on small crustaceans and other invertebrates (*1*). By swimming in a tight circle on the water surface, they generate a vortex that draws underlying fluid and suspended prey toward the surface (*2*). By pecking on the water surface at a rate of ~1.5 Hz (*1*, *3*–*6*), the birds capture water droplets with a characteristic scale of ~2 mm between their upper and lower mandibles (movie S1). Suction cannot be used to raise the drops mouthward because of the geometry of the open beak; gravity acts to oppose the drop motion. Nevertheless, the birds succeed in raising the drops mouthward by opening and closing their beaks successively (*1*, *5*, *7*, *8*). Although the importance of surface tension in this process was inferred (*1*), the physical mechanism responsible for the droplet transport, specifically

[1]Center for Bits and Atoms, Massachusetts Institute of Technology (MIT), 20 Ames Street, Cambridge, MA 02139, USA. [2]Physique et Mécanique des Milieux Hétérogènes, UMR 7636 du CNRS, Ecole Supérieure de Physique et de Chimie Industrielles, 10 rue Vauquelin, 75005 Paris, France. [3]Department of Mathematics, MIT, 77 Massachusetts Avenue, Cambridge, MA 02139, USA.

the critical role of the beak's characteristic tweezering action, has yet to be rationalized.

When a fluid drop is placed on a flat solid, the equilibrium contact angle θ between the wetted solid surface and the interface is defined by the well-known Young's equation. If $\theta \to 0$, the drop completely wets the solid, whereas for any finite θ, the drop is said to partially wet the solid. In practice, static contact angles observed in the case of partial wetting may lie anywhere in a finite range bounded above and below by the values at which contact line motion is initiated; specifically, the advancing and receding contact angles, respectively θ_a and θ_r (*9*–*11*). An important consequence of this so-called contact-angle hysteresis is a contact force that causes drops to adhere to surfaces; for example, rain drops stick to window panes because of the difference in the contact angles on their upper and lower edges (*12*). Although contact-angle hysteresis typically acts to resist the sliding of droplets on solids (*10*, *11*), it may be overcome by vibration (*13*, *14*). We demonstrate that, in capillary feeding, contact-angle hysteresis couples to the time-dependent beak geometry corresponding to the mandibular spreading cycles (*1*, *5*–*8*), thereby driving drop motion via a ratcheting mechanism.

Surface tension transport relies explicitly on the bird opening and closing its beak and so varying the beak opening angle α (*1*, *5*) (Fig. 1B). This angle has an upper bound because a drop pinned between two plates will break at an opening angle α_{break} if its height-to-radius ratio exceeds 2π (*15*–*17*). Denoting the beak length by L_b and the drop size by the capillary length $l_c \sim (\gamma/\rho g)^{1/2} \sim 2$ mm (where γ is surface tension, ρ is density, and *g* is the gravitational acceleration), the maximum opening angle is thus on the order of $\alpha_{break} \sim l_c/L_b \sim 11°$ for capillary feeders (Fig. 1B and fig. S1). The characteristic time to transport a drop along the beak length $L_b \sim 2$ cm is 20 ms, corresponding to mean drop speeds as high as 100 cm/s (*1*, *4*). In Fig. 1B, we present the mean beak length and width of 18 shorebird species with straight bills and emphasize that surface tension transport is used only by birds with the smallest beaks. Rubega (*3*) demonstrated that beak dimensions do not scale with body size in adult red-necked phalaropes, *Phalaropus lobatus*, suggesting the critical role of beak morphology in capillary feeding. Recently, Estrella *et al*. (*5*) substantially expanded the list of capillary feeders (Fig. 1B), underscoring the prevalence of surface tension transport. Though morphometric analysis of bird bills commonly yields insight into foraging mechanisms (*18*) and has led to new understanding of feeding modes (*19*), analytical and experimental studies of these mechanisms are exceedingly rare (*20*). We here present one such study.

In our experimental study, we constructed mechanical wedgelike geometries modeled after the bird beak. Mechanical beaks with a stainless steel surface were polished with a Buehler Metadi diamond slurry (average particle size ~ 3 μm). The surface was ultrasonically cleaned for an hour, plasma-treated in oxygen for 1 min to remove any residue, then left in air for an hour before experiments were performed. The mechanical beaks were mounted and actuated by a motorized micrometer stage so that the beak opening and closing angle could be precisely controlled by a computer. Drops of known volume (ranging from 0.5 to 2 μl) were inserted via a micropipette at the tip of the beak. A high-speed video camera (Phantom v5.0) recorded the resulting drop dynamics.

We first deposited a completely wetting fluid (silicone oil, $\gamma = 0.02$ N/m) in the form of a droplet that spanned the wedge (Fig. 2A). The drops propagated toward the narrower region, advancing first at a constant speed then accelerating as they approached the apex of the wedge (Fig. 2, B and C). The behavior in this fully wetting regime may be rationalized by simple scaling arguments (supporting online material). The jump in pressure across a surface is proportional to γ and the local curvature; such curvature pressures are capable of driving fluid motion. In 1712, Hauksbee (*21*) reported that "oil of orange" droplets trapped between two nonparallel glass plates moved spontaneously in the direction of decreasing gap thickness. Similarly, a completely wetting fluid drop confined in a conical capillary is known to self-propel toward the narrower end because of the axial force arising from differing curvature pressures across its end caps (*22*). In our wedge geometry, the opening angle is denoted by α, the width of the drop by *W*, the distance of the drop from the apex by *x*, and the length of the drop by *L* (Fig. 2B). The drop height is necessarily α*x*. For $x > L$, the pressure difference between the two caps scales

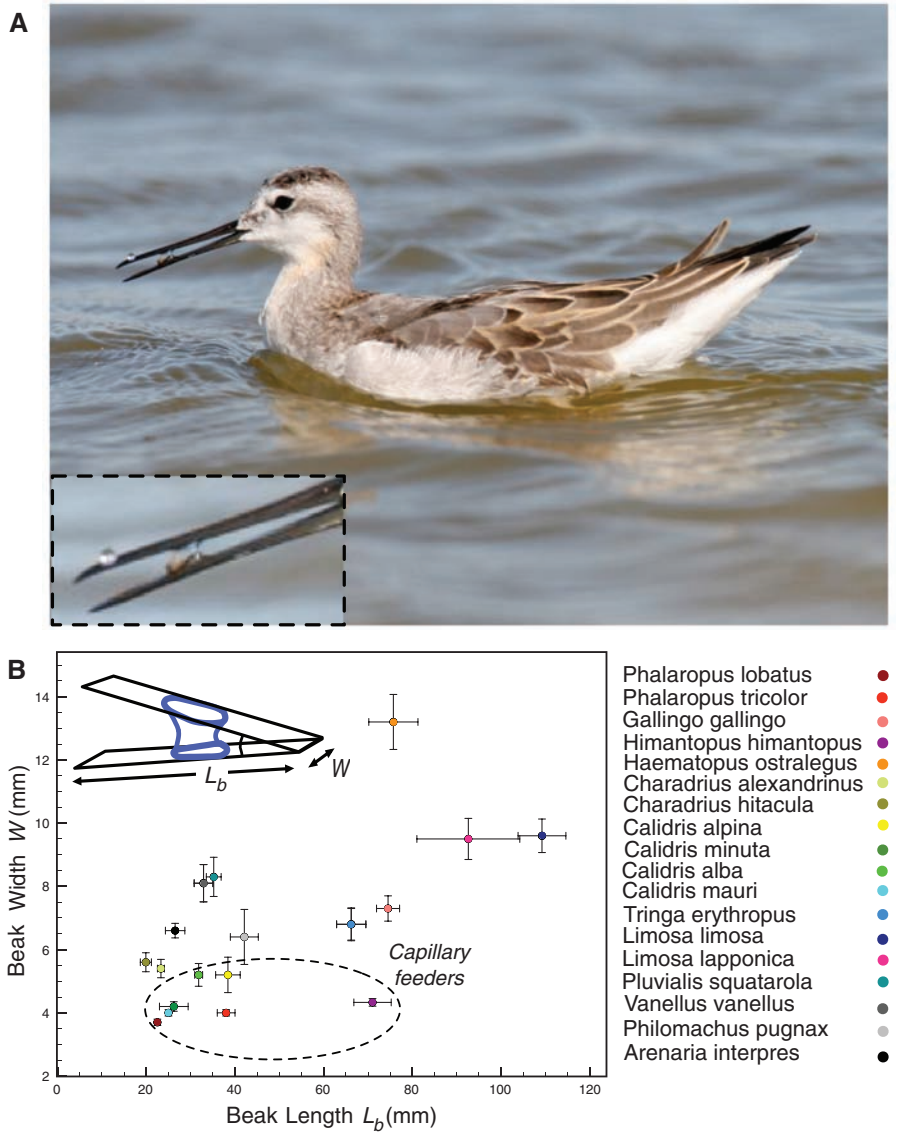

Fig. 1. (**A**) A juvenile Wilson's phalarope feeding. Note the prey suspended in the droplet trapped in its beak (inset). [Photo courtesy of Robert Lewis] (**B**) Shorebirds use a variety of foraging strategies (*28*) and so exhibit large variations in beak size and shape. Here we plot the bill length and base width of common shorebirds with straight bills [data compiled from (*4*, *18*, *29*)]. Scale bars represent the standard deviation in the reported data.

as $\gamma L/\alpha x^2$ and the drop volume as $\Omega \sim \alpha x L W$; hence a driving force $F \sim \gamma W L/x$ arises. For a fluid drop with dynamic viscosity η advancing at a speed v, the viscous force resisting its motion is given by $F_\eta \sim \eta W L v/(\alpha x)$; the force balance thus yields a steady speed $v_0 \sim \gamma\alpha/\eta$ that is independent of drop position x and drop length L. As the drop approaches the apex, $x < L$, the pressure difference between the caps scales as $\gamma/(\alpha x)$ and the volume as $\alpha L^2 W$. The resulting driving force now varies as $\gamma L W/x$, and the viscous resistance as $\eta W v/\alpha$. The resulting drop speed $v_0 L/x$ diverges as the drop approaches the apex despite the progressively increasing confinement. After a brief transient period, these two distinct regions of constant speed and acceleration are apparent in Fig. 2C.

When water is used in place of oil, the behavior is strikingly different: No droplet motion arises (Fig. 3A, top row). Unlike the silicone oil, the water only partially wets the solid; consequently, the droplet motion is resisted by contact-angle hysteresis. Specifically, there is an adhesive force whose magnitude scales as $\gamma W \Delta\cos\theta$, where $\Delta\cos\theta = \cos\theta_r - \cos\theta_a$ (*10*, *23*), and W is the length of the advancing contact line. In our system, water droplets on stainless steel beaks have an advancing angle $\theta_a \sim 65°$ and receding angle $\theta_r \sim 20°$ that are comparable to those of water droplets on keratin (*24*). Drop motion is possible only if the capillary driving force $F \sim \gamma\cos\theta\ (WL/x)$ exceeds this sticking force; that is, if $\alpha > [(\Delta\cos\theta)/\cos\theta]\ [\Omega/(WL^2)]$. This condition cannot be satisfied, because both $\Delta\cos\theta/\cos\theta$ and $\Omega/(WL^2)$ are order-one quantities, whereas α must be less than $\alpha_{break} \sim 0.2$ radians for drop stability. The relatively minor influence of the fully three-dimensional geometry was examined numerically (fig. S1). The influences of beak taper and orientation were examined both experimentally and numerically. Realistic beak tapers (*3*, *5*) were found to have only a weak quantitative effect on the drop propulsion, whereas beak orientation had a negligible effect in the ratcheting regime.

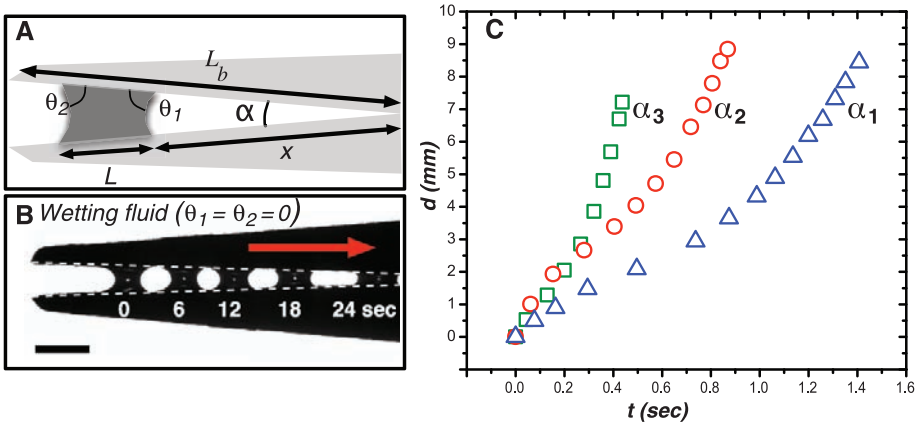

Fig. 2. Fluid drop in a horizontal beak. (**A**) Schematic of a bird beak with a fluid drop trapped between upper and lower mandibles. (**B**) A completely wetting drop of silicone oil ($\theta_1 = \theta_2 = 0$, dynamic viscosity $\eta = 0.05$ kg m^{-1} s^{-2}) self-propels toward the apex of a mechanical bird beak with a constant opening angle $\alpha = 3.4°$ and uniform width of 1 mm. Scale bar, 2 mm. (**C**) Plot of drop front position versus time for silicone oil ($\eta = 0.01$ kg m^{-1} s^{-2}) for three opening angles $\alpha_1 = 1.9°$ (blue triangles), $\alpha_2 = 2.8°$ (red circles), and $\alpha_3 = 4.2°$ (green squares), where d (in millimeters) represents the distance from the beak tip to the drop's trailing edge.

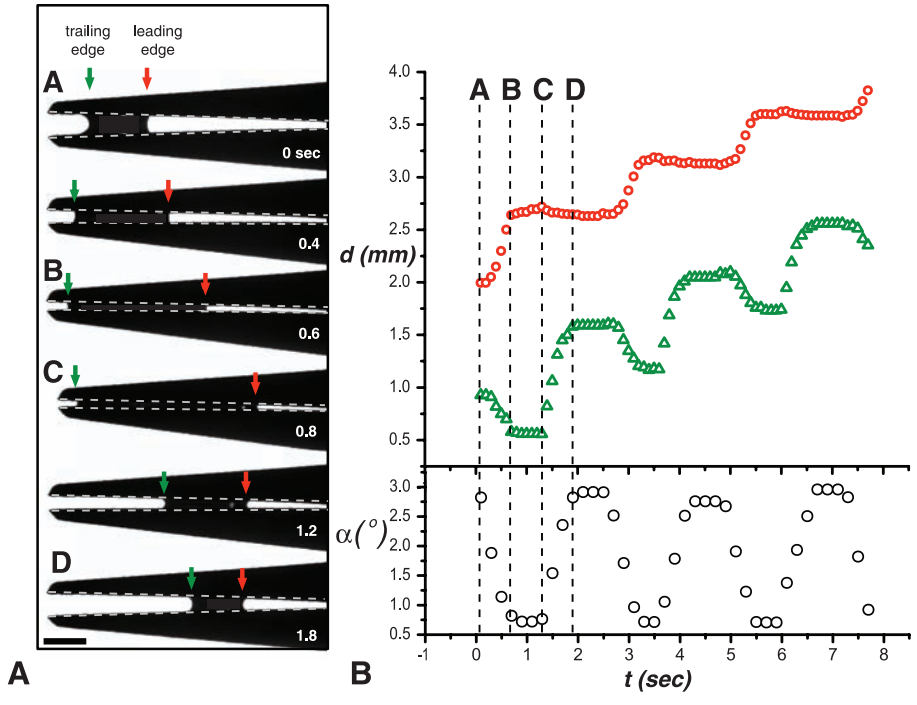

Fig. 3. The capillary ratchet. (**A**) Time sequence illustrating the water droplet transport generated by an opening and closing cycle of the mechanical beak. In the closing cycle, the leading contact line proceeds toward the mouth; in the opening cycle, the trailing contact line recedes toward the mouth. The result is net drop transport toward the mouth. Scale bar, 2 mm. (**B**) Plot of the associated motion of the leading (red) and trailing (green) contact lines generated by varying the opening angle α over three cycles. d (in millimeters) represents the distance from the beak tip to the contact line. [See also movie S2]

Phalaropes induce drop motion by cyclically opening and closing their beaks (*1*). We followed their lead in actuating the mechanical beak by opening and closing the wedge geometry at a constant angular velocity ω, with α_{close} and α_{open} being the minimum and maximum opening angles, respectively. We recorded the location of both front and rear contact lines of the drop with a high-speed camera mounted on a microscope (Fig. 3A). For a given drop volume, varying α_{close} and α_{open} reveals three distinct regimes.

If $\alpha_{open} - \alpha_{close}$ is sufficiently small that the leading and trailing contact angles, θ_1 and θ_2 respectively, satisfy $\theta_r < \theta_2 < \theta_1 < \theta_a$, then the drop remains pinned (Fig. 4A). The dynamics for larger values of $\alpha_{open} - \alpha_{close}$ are best understood by considering in turn the closing and opening phases. During the closing phase, both contact lines have the tendency to progress outward, but the leading edge (A) always does so first. During the opening phase, both contact lines tend to retreat inward, but the trailing edge (B) does so first. The drop thus advances through a slipping ratcheting motion: In each cycle, both leading and trailing edges of the contact lines advance and retreat. Nevertheless, due to the asymmetry in the wedge geometry, net mouthward drop motion is still achieved, albeit inefficiently. When α_{close} and α_{open} are optimally tuned, the droplet advances through a pure ratcheting motion with no slippage. The two contact lines move asynchronously but progressively toward the apex: During the opening phase, the leading edge (B) remains pinned while the trailing edge (A) retreats; during closing, the leading edge (B) advances while the trailing edge (A) remains pinned (Fig. 4A). The time dependence of the contact line positions and opening angle for nearly pure capillary ratcheting is plotted in Fig. 3B. The ratcheting motion is quasi-static, with the instantaneous position of the drop being determined by the history of the beak motion; therefore, the

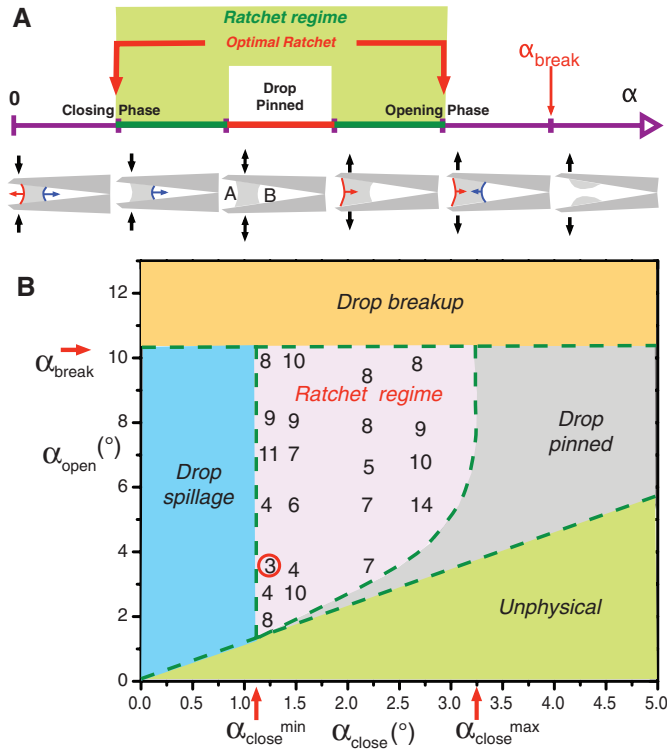

Fig. 4. (**A**) A schematic illustration of droplet dynamics in an oscillating bird beak. The drop is pinned for region $\theta_a > \theta_1 > \theta_2 > \theta_r$, marked by the red line. As the beak is closed progressively, first the leading (A) then the leading and trailing (B) contact lines advance. As the beak is opened, first the trailing (B) then the trailing and leading (A) contact lines retreat. Ultimately, the drop breaks when $\alpha > \alpha_{break}$. The ratcheting regime is indicated in green and the optimal ratchet by the red arrows. (**B**) Regime diagram for droplet transport in an oscillating mechanical bird beak illustrates the dependence of the system's behavior on the minimum and maximum opening angles α_{close} and $\alpha_{open} > \alpha_{close}$, respectively. The drop volume was fixed at 1.5 μl. For $\alpha_{open} > \alpha_{break}$, the drop breaks, whereas for $\alpha_{close} < \alpha_{close}^{min}$, the drop spills from the beak. The numbers denote the number of cycles required to transport the drop from the beak tip to the mouth in the ratcheting regime. The optimal capillary ratchet transports the drop in three cycles.

drop speed increases linearly with the ratcheting frequency ω.

Figure 4B illustrates the various regimes of droplet transport observed in our mechanical bird beak when the minimum and maximum opening angles, α_{close} and α_{open}, respectively, were varied. In addition to regimes characterized by drop pinning and drop breakup, we report the number of cycles required for drop transport from the mechanical beak tip to the apex of the wedge in the ratchet regime. For our specific combination of droplet volume (1.5 μl) and mechanical beak geometry, the minimum number of cycles, three, corresponds to the most efficient capillary ratchet. It is interesting to speculate as to the degree of optimization of capillary feeding in the wild. On average, a single drop is transported from the beak tip to the buccal cavity of the red-necked phalarope in two to three mandibular spreading cycles (*1*, *4*). Wilson's phalaropes are evidently less optimized for capillary feeding, and require seven to eight cycles (*7*). Our observations provide a quantitative measure of the efficiency of shorebird beaks in capillary feeding, and so may yield insight into their degree of adaptation. Moreover, they yield new insight into recent observations of rynchokinesis, in which capillary feeding may be enhanced by beak flexure (*6*).

The beaks of shorebirds may be largely vertical during capillary feeding; thus, the influence of gravity needs to be considered. Although gravity acts to resist the climbing drop, it is overcome by contact-angle hysteresis provided that the pinning force, $F_p = \gamma W \Delta \cos\theta$, exceeds the drop and prey weight, Mg. Characteristic values for the phalarope [$W \sim 2$ mm, $\Omega \sim 5$ to 10 μl (*1*)] indicate that $F_p/(Mg) > 1$: Contact-angle hysteresis can safely support the drop's weight. In our experimental study, changing the orientation of the mechanical beaks from horizontal to vertical indeed had a negligible effect on the dynamics of the water drops. Conversely, wetting silicone droplets were observed to slip downward under the influence of gravity, owing to the absence of contact-line pinning. Wetting droplets would slip if the propulsive capillary force $\gamma WL/x$ were exceeded by the drop's weight. Because the relative magnitudes of these forces are given by $l_c^2/(\alpha L_b^2) \sim 0.1$, with $\alpha \sim 5° = 0.1$ rad and beak length $L_b \sim 2$ cm, we conclude that gravity would preclude capillary feeding if the beaks were wetting. We thus see that, although the partially wetting nature of the bird beaks disables static capillary propulsion through the introduction of an adhesive force, it enables droplet transport via capillary ratcheting, a mechanism that naturally overcomes gravity. We thus highlight the precarious nature of capillary feeding: Any surface contamination that alters the wetting properties of the beaks represents a serious threat, particularly to shorebirds such as the red-necked phalarope that rely exclusively on this mode of feeding (*1*). Given the drastic changes in wetting behavior that accompany contamination with pollutants such as petroleum or detergents (*23*), our study makes clear the critical danger posed to this class of shorebirds by chemical or oil spills (*25*, *26*).

Contact-angle hysteresis typically resists the motion of drops on solid substrates; conversely, in capillary feeding, it couples with the time-dependent beak geometry to drive the drops. As such, surface tension transport represents a peculiarity for which contact-angle hysteresis enables rather than impedes drop motion. By elucidating the dependence of the efficiency of the capillary ratchet on dynamic beak morphology, we have enabled quantitative comparative studies of capillary feeding across species. The efficiency of capillary feeding may be enhanced by tuning the beak geometry, dynamics, and wetting properties. Analogous mechanisms for small-scale drop transport in microfluidic systems (*27*) are currently being explored.

References and Notes

1. M. A. Rubega, B. S. Obst, *Auk* **110**, 169 (1993).
2. B. S. Obst *et al.*, *Nature* **384**, 121 (1996).
3. M. A. Rubega, *J. Morphol.* **228**, 45 (1996).
4. M. A. Rubega, thesis, University of California, Irvine, CA (1993).
5. S. M. Estrella, J. A. Masero, A. Perez-Hurtado, *Auk* **124**, 1244 (2007).
6. S. M. Estrella, J. A. Masero, *J. Exp. Biol.* **210**, 3757 (2007).
7. M. A. Rubega, *Ibis* **139**, 488 (1997).
8. G. Zweers, *Acta Biotheor.* **39**, 15 (1991).
9. F. Brochard, *Langmuir* **5**, 432 (1989).
10. P. G. de Gennes, *Rev. Mod. Phys.* **57**, 827 (1985).
11. R. H. Dettre, R. E. Johnson, *Contact Angle, Wettability, and Adhesion*, vol. 43 of *Advances in Chemistry Series* (American Chemical Society, Washington, DC, 1964).
12. E. Dussan, R. T. P. Chow, *J. Fluid Mech.* **137**, 1 (1983).
13. S. Daniel, M. K. Chaudhury, *Langmuir* **18**, 3404 (2002).
14. S. Daniel, M. K. Chaudhury, P.-G. de Gennes, *Langmuir* **21**, 4240 (2005).
15. T. Y. Chen, J. Tsamopoulos, R. J. Good, *J. Colloid Int. Sci.* **151**, 49 (1992).
16. B. J. Lowry, P. H. Steen, *Proc. R. Soc. London Ser. A* **449**, 411 (1995).
17. P. Concus, R. Finn, *Phys. Fluids* **10**, 39 (1998).
18. S. Nebel, D. Jackson, R. Elner, *Anim. Biol.* **55**, 235 (2005).
19. R. W. Elner, P. G. Beninger, D. L. Jackson, T. M. Potter, *Mar. Biol.* **146**, 1223 (2005).
20. S. Humphries, R. H. C. Bonser, M. P. Witton, D. M. Martill, *PLoS Biol.* **5**, 1647 (2007).
21. F. Hauksbee, *Philos. Trans.* **27**, 395 (1712).
22. H. Bouasse, *Capillarité et Phénomènes Superficiels* (Librairie Delagrave, Paris, 1924).
23. P. G. de Gennes, F. Brochard-Wyart, D. Quéré, *Capillarity and Wetting Phenomena: Drops, Bubbles, Pearls and Waves* (Springer-Verlag, Berlin, 2003).
24. Y. K. Kamath, C. J. Dansizer, H. Weigmann, *J. Appl. Polym. Sci.* **22**, 2295 (1978).
25. Z. A. Eppley, M. A. Rubega, *Nature* **340**, 513 (1989).
26. R. Stephenson, *Environ. Conserv.* **24**, 121 (1997).
27. M. Prakash, N. Gershenfeld, *Science* **315**, 832 (2007).
28. A. Barbosa, E. Moreno, *Auk* **116**, 712 (1999).
29. T. Szekely, R. P. Freckleton, J. D. Reynolds, *Proc. Natl. Acad. Sci. U.S.A.* **101**, 12224 (2004).

30. J.B. acknowledges support from NSF. M.P. acknowledges support from the MIT Center for Bits and Atoms (NSF grant CCR-0122419). A patent on the use of contact-angle hysteresis for the directed transport of fluid droplets, relevant to microfluidic technologies, has been filed by MIT.

Supporting Online Material

www.sciencemag.org/cgi/content/full/320/5878/931/DC1
SOM Text
Figs. S1 and S2
Movies S1 and S2

4 February 2008; accepted 24 March 2008
10.1126/science.1156023